Selective localization of hierarchically assembled particles to plasma membranes of living cells

Asish C Misra[1,2], Tae-Hong Park[3,4], Randy P. Carney[5,6], Giulia Rusciano[7], Francesco Stellacci[5,6] & Joerg Lahann[1,3]

[1]Department of Biomedical Engineering, University of Michigan, Ann Arbor, MI, USA, [2]Current address: Department of Surgery, Beth Israel Deaconess Medical Center, Boston, MA, USA, [3]Department of Chemical Engineering, University of Michigan, Ann Arbor, MI, USA, [4]Current address: Korea Atomic Energy Research Institute, Daejeon, Republic of Korea, [5]Institute of Materials, École Polytechnique Fédérale de Lausanne, Switzerland, [6]Interfaculty Institute of Bioengineering, École Polytechnique Fédérale de Lausanne, Switzerland, [7]Dipartimento di Fisica "Ettore Pancini" Università di Napoli "Federico II". Correspondence should be addressed to J. L. (lahann@umich.edu).

Keywords: nanoparticles, subcellular targeting

Particles that preferentially partition to a specific cellular subunit, such as the nucleus, mitochondria or the cytoskeleton, are of relevance to a number of applications, including drug delivery, genetic manipulation, or self-assembly. Here, we present hierarchical assemblies of fully synthetic particles that selectively localize to the plasma membrane of mammalian cells. We have used a multimodal approach to create assemblies of polymer-based carrier particles with amphiphilic gold nanoparticles immobilized on one hemisphere. These assemblies persist in the plasma membrane of cells for several days and undergo rearrangements and clustering, typically considered to be hallmarks of membrane-bound receptors.

This is the author manuscript accepted for publication and has undergone full peer review but has not been through the copyediting, typesetting, pagination and proofreading process, which may lead to differences between this version and the Version of Record. Please cite this article as doi: 10.1002/smtd.201800408.

From drug-loaded nanocarriers to prosthetic implants, a number of materials have been designed to interface with biological systems at different length scales. [1-6] (Niinomi 2002, Liu, Chu et al. 2004, Alarcon, Pennadam et al. 2005, Neuberger, Schopf et al. 2005, Dykman and Khlebtsov 2012, Li, Barnes et al. 2012) (Niinomi 2002, Liu, Chu et al. 2004, Alarcon, Pennadam et al. 2005, Neuberger, Schopf et al. 2005, Dykman and Khlebtsov 2012, Li, Barnes et al. 2012) [1-6] Of particular interest is the development of particulate materials that draw their characteristic function from interactions at the cellular and subcellular level, with applications including targeted drug delivery, tissue engineering, or self-assembly. [7-10] (Soppimath, Aminabhavi et al. 2001, Cho, Wang et al. 2008, Nie, Petukhova et al. 2010, Shi, Votruba et al. 2010) (Soppimath, Aminabhavi et al. 2001, Cho, Wang et al. 2008, Nie, Petukhova et al. 2010, Shi, Votruba et al. 2010) [7-10] Nature displays a range of biological structures capable of interfacing with and penetrating through cell membranes, including structures for selective fusion into cellular membranes. [11-15] (Hoekstra and Kok 1989, Lidmar, Mirny et al. 2003, Glotzer, Horsch et al. 2005, Douglas and Young 2006, Glotzer and Solomon 2007) (Hoekstra and Kok 1989, Lidmar, Mirny et al. 2003, Glotzer, Horsch et al. 2005, Douglas and Young 2006, Glotzer and Solomon 2007) [11-15]

A number of methods exist for the fabrication of particles with complex architectures which may be used to mimic naturally occurring intricate structures. [16,17] (Lee, Yoon et al. 2011, Yoon, Lee et al. 2011) (Lee, Yoon et al. 2011, Yoon, Lee et al. 2011) [16,17] For instance, electrohydrodynamic (EHD) co-jetting allows for rapid fabrication of particles with complex architectures. [17-33] (Roh, Martin et al. 2005, Roh, Martin et al. 2006, Roh and Lahann 2007, Roh, Yoshida et al. 2007, Roh, Yoshida et al. 2007, Yoshida, Roh et al. 2007, Bhaskar, Roh et al. 2008, Yoshida, Roh et al. 2009, Bhaskar, Pollock et al. 2010, Lee, Yoon et al. 2011, Lee, Yoon et al. 2012, Misra, Bhaskar et al. 2012, Saha, Copic et al. 2012, Gao and Yu 2013, Sarangi and Patnaik 2014, Li, Wang et al. 2015, Bartolami, Bouillon et al. 2016) (Roh, Martin et al. 2005, Roh, Martin et al. 2006, Roh and Lahann 2007, Roh, Yoshida et al. 2007, Roh, Yoshida et al. 2007, Yoshida, Roh et al. 2007, Bhaskar, Roh et al. 2008, Yoshida, Roh et al. 2009, Bhaskar, Pollock et al. 2010, Lee, Yoon et al. 2011, Lee, Yoon et al. 2012, Misra, Bhaskar et al. 2012, Saha, Copic et al. 2012, Gao and Yu 2013, Sarangi and Patnaik 2014, Li, Wang et al. 2015,

Bartolami, Bouillon et al. 2016) [17-33] Compared to conventional electrospraying, EHD co-jetting involves extrusion of two or more polymer solutions through a nozzle under a laminar flow regime (**Fig. S1**). Upon application of a DC voltage, the droplet becomes distorted and forms a Taylor cone, from which a high-speed jet is produced. [34,35] (Ganan-Calvo 1997, Luedtke, Landman et al. 2008) (Ganan-Calvo 1997, Luedtke, Landman et al. 2008) [34,35] Modification of process and solution parameters may lead to a variety of bi- and multicompartmental particles with controllable shape and size. [21,36] (Bhaskar, Pollock et al. 2010, Lahann 2011) (Bhaskar, Pollock et al. 2010, Lahann 2011) [21,36] Due to the laminar flow of the jetting solutions, the interface between solutions is conserved throughout the process leading to the formation of multicompartmental particles. [21,26,27] (Roh, Martin et al. 2005, Roh, Martin et al. 2006, Bhaskar, Pollock et al. 2010) (Roh, Martin et al. 2005, Roh, Martin et al. 2006, Bhaskar, Pollock et al. 2010) [21,26,27]

Because of the establishment of distinct compartments, the particle surface can be chemically modified in ways that lead to distinct patterns. [19,22,26,29] (Roh, Martin et al. 2005, Bhaskar, Roh et al. 2008, Yoshida, Roh et al. 2009, Saha, Copic et al. 2012) (Roh, Martin et al. 2005, Bhaskar, Roh et al. 2008, Yoshida, Roh et al. 2009, Saha, Copic et al. 2012) [19,22,26,29] Selective surface modification of particle patches has been demonstrated using several different chemistries, including orthogonal click reactions. [19,29] (Bhaskar, Roh et al. 2008, Saha, Copic et al. 2012) (Bhaskar, Roh et al. 2008, Saha, Copic et al. 2012) [19,29] A variety of molecules including polymers, dyes and peptides have been selectively conjugated to a surface patches resulting in directed interactions with mammalian cells. [26] (Roh, Martin et al. 2005) (Roh, Martin et al. 2005) [26] Our overarching hypothesis is that an appropriate balance of repulsion and membrane affinity will result in selective localization of hierarchically assembled particles onto plasma membranes.

To tune the interactions of particles with the cell membrane, gold nanoparticles coated with a mixture of 1-octanethiol (OT) and 11-mercaptoundecanesulfonic acid (MUS) are of particular interest, because they have previously been reported to penetrate cell membranes through energy-independent pathways. [37-40] (Verma, Uzun et al. 2008, Van Lehn, Ricci et al. 2014, Yang, Carney et al. 2014,

Atukorale, Yang et al. 2015) (Verma, Uzun et al. 2008, Van Lehn, Ricci et al. 2014, Yang, Carney et al. 2014, Atukorale, Yang et al. 2015) [37-40] OT, a hydrophobic ligand, and MUS, a hydrophilic ligand, are organized in a "striped" fashion on the surface of the gold nanoparticles.[37] This particular arrangement of ligands affords the particles the ability to penetrate through cell membranes and enter cells without the need for internalization via an endocytic mechanism.[37] This property has been further confirmed by experiments and by theoretical work elucidating the fundamental interactions of these particles with lipid bilayers. [38,41] (Van Lehn, Atukorale et al. 2013, Van Lehn, Ricci et al. 2014) (Van Lehn, Atukorale et al. 2013, Van Lehn, Ricci et al. 2014) [38,41] From simulations it has been shown that the gold nanoparticles within the bilayer is a thermodynamically favorable state (minimized exposure of hydrophobic ligands on nanoparticles to water) which is thought to be achieved by stochastic protrusion of an aliphatic lipid tail into solution.[38]

In this paper, we use chemically functionalized multicompartmental particles to create carrier systems with two distinct surface patches: (i) one hemisphere is modified with PEG to reduce non-specific interactions; (ii) one hemisphere is decorated with MUS:OT gold nanoparticles to impart affinity towards the plasma membrane of mammalian cells.

First, we prepared bicompartmental particles containing two different chemically reactive polymers that can undergo reactions orthogonal to one another (**Fig. S1**). The particles were prepared via EHD co-jetting of two different polymer solutions of polyacrylamide/poly(acrylic acid) co-polymers (PAAm-*co*-AA) containing PAAm-*co*-AA modified with acetylene groups[22](Yoshida, Roh et al. 2009)(Yoshida, Roh et al. 2009)[22] in one side and dextran modified with amine groups, amino-dextran, in the other. These functional polymers enabled subsequent surface functionalization via chemical coupling reactions. Fluorescein isothiocyanate (FITC)- and rhodamine-conjugated dextrans were further added to the respective jetting solutions to enable characterization of the particle compartmentalization using confocal laser scanning microscopy (CLSM). [25] (Roh, Yoshida et al. 2007) (Roh, Yoshida et al. 2007) [25]

The hierarchical assembly of individual particles was achieved by first conjugating PEG onto one hemisphere. For this purpose, amine groups were reacted with *N*-hydroxylsuccinimide-functionalized polyethylene glycol (PEG-NHS). Then, the acetylene groups presented on the second hemisphere were selectively conjugated with azide-functionalized MUS:OT gold nanoparticles via Huisgen 1,3-dipolar cycloaddition. MUS:OT gold nanoparticles, 5 nm in diameter, coated with a 2:1 stoichiometric mixture of OT and MUS were synthesized with a one-phase method. [37] (Verma, Uzun et al. 2008) (Verma, Uzun et al. 2008) [37] Azide-terminated thiol ligands were then place-exchanged on the particles with a protocol that typically leads to ~10-20 ligands per particles. [37] (Verma, Uzun et al. 2008) (Verma, Uzun et al. 2008) [37] This surface modification approach resulted in particles that were decorated with MUS:OT gold nanoparticles on one hemisphere and PEG molecules on the remaining hemisphere, denoted as cell membrane-localized particles (CMLPs; **Fig. 1a**). The bicompartmental architecture of the particles was intact throughout the surface modification, as confirmed by CLSM (**Fig. 1b**). Since the acetyl-functionalized copolymer and amino-dextran were localized in their respective compartments, the surface-functionalization of these particles was specific, as confirmed by transmission electron microscopy (TEM). TEM images of the fully assembled carrier particles revealed the preferential localization of the gold nanoparticles on one hemisphere (**Fig. 1c**). For comparison, we also synthesized a reference particle, "Control," (**Fig. 1a**), which was identical to the active particles, CMLPs, except, that the surface-bound gold nanoparticles were coated only with MUS, lacking the unique display of MUS and OT.

To elucidate the *in vitro* behavior of CMLPs, we incubated breast cancer cells that constitutively express green fluorescent protein, MDA-MB-231/GFP, for 6 hours with CMLPs. The CMLPs were compared to the control particles, and CLSM analysis was used to assess the cell binding capacity of the particle formulations. Representative images are shown in **Fig. 2a** and reveal that the level of binding was higher for the CMLPs compared to the control particles. Quantification of the number of particles per cell (**Fig. 2b**) suggested that significantly more particles were bound to the cancer cells for the CMLP group than the control group. The maximum binding achieved by the controls was 1.7

± 0.1 particles per cell for the highest incubation concentration of 100 μg/ml, while 5.3 ± 0.1 CMLPs were bound per cell at the lowest incubation concentration of 10 μg/ml.

To further assess differences in particle internalization, additional studies were performed, staining endosomes with a blue fluorescent dye (Lysotracker) followed by a 6-hour incubation. [42] (Panyam, Sahoo et al. 2003) (Panyam, Sahoo et al. 2003) [42] This procedure allowed us to identify particles in the cell interior, distinguishing between membrane-bound and endocytosed particles. In **Fig. 3a**, the CLSM images of control particles reveal that the particle fluorescence overlaps with the blue fluorescence from the endosomes (orange arrows), suggesting that these particles are internalized via endocytosis. On the other hand, CMLPs (red arrows) localized outside of endosomes (yellow arrows). Further examination using 3D reconstructions of confocal images verified that the control particles were internalized, while a significant fraction of the CMLPs was localized to the plasma membrane (**Fig. S2**). These observations were also independently validated by SEM (**Fig. 3b)** – for the control, generally 1-2 particles were found per individual cell surface, whereas as many as 10 CMLPs were localized on an individual cell surface. There is therefore a significant cell-membrane localizing effect associated with the particles with surface-bound amphiphilic gold nanoparticles. This effect may be in part enhanced or elucidated due to markedly reduced nonspecific interactions, primarily endocystosis, by PEGylation, as validated by incubation of unmodified, as-jetted particles and PEGylated particles shown in **Fig. S3**.

Next we wanted to understand the longer-term behavior of the cell membrane binding of CMLPs. We therefore extended the incubation times to 24, 48, and 72 hours (**Fig. 4**). At no time point did we observe appreciable cell death, suggesting that these particles were biocompatible under the experimental conditions. Quantification of this data is shown in **Fig. S4**. For incubation times greater than 6 hours, we observed that the control particles remained confined in endosomes. From 24 to 72 hours, more of the control particles were endocytosed. While we also observed an increase in the endocytosed fraction of CMLPs after 72 hours, the majority of the membrane-associated CMLPs rearranged into aggregates that appeared to form specific domains on the cell membrane. To

quantitatively analyze the clustering of CMLPs, a K-means analysis was performed based on particle locations determined by red fluorescent confocal images (**Fig. 5a**). There was a fivefold increase of CMLPs found in each cluster compared to the control particles (**Fig. 5b**). Additionally, the average radius of each CMLPs cluster was larger than for the control groups (**Fig. 5c**). The clustering of the CMLPs persisted over the entire period of the experiment revealing a profoundly distinct clustering behavior compared to all control particles. The CMLPs may further associate and cluster on the cell membrane, as it may be a more thermodynamically favorable state. Each CMLP associating to the membrane may decrease the overall binding energy, similar to the receptor clustering of cell membranes. [43,44] (Bray, Levin et al. 1998, Gajate and Mollinedo 2005) (Bray, Levin et al. 1998, Gajate and Mollinedo 2005) [43,44] Hence, CMLPs dispersed in the medium are more likely to bind to these lower energy areas and direct particle clustering over time. However, further studies would be required to demonstrate such a mechanism.

While the exact mechanism of selective localization of CMLPs and their long-term behavior require further studies to elucidate, these current studies suggest that the local interaction of MUS:OT gold nanoparticles with the cellular membrane appears to be a contributory factor. Therefore, to further our understanding of the nature and the effects of such interaction, giant unilamellar vesicles (GUVs), [45] (Richmond, Schmid et al. 2011) (Richmond, Schmid et al. 2011) [45] typically used to study membrane organization and response to external agents, were employed as a model of cellular membranes. In particular, GUVs based on 1,2-dioleoyl-sn-glycero-3-phosphocholine (DOPC-GUVs), mimicking the fluid phase of real eukaryotic membranes, were used. The study was performed with a Raman-tweezers system, where a Raman microscope was combined with an optical tweezers system, [46] (Dholakia and Cizmar 2011) (Dholakia and Cizmar 2011) [46] that provides access to both the micromechanical and the chemical effect of NPs on the optically trapped GUVs, free from spurious surface-induced artifacts.

Initially, the chemical effect of the MUS:OT gold nanoparticles on the GUVs was investigated. GUVs were studied with the micro-Raman system, after being exposed to different gold nanoparticle

concentrations, ranging from 0.01 mg/ml to 10 mg/ml. Above a concentration of 1 mg/ml, a significant number of GUVs spectra exhibited clearly discernable signatures of Raman bands which were attributed to the presence of the MUS:OT gold nanoparticles, as seen in **Fig. 6a**. Intriguingly, the intensity changes of these bands among different GUVs appear to be normally distributed (**Fig. 6b**), suggesting a randomized interaction process between nanoparticles and the lipid bilayer, which is consistent with their amphiphilic character. This localization effect was not observed for GUVs incubated with gold nanoparticles coated only with MUS, under otherwise identical experimental conditions.

Next, the micromechanical properties of GUVs upon interaction with the amphiphilic gold nanoparticles were investigated. It is known that the insertion of rigid proteins or peptides into membranes typically results in the stiffening of the lipid bilayer. [47] (Schulz, Olubummo et al. 2012) (Schulz, Olubummo et al. 2012) [47] In our study, the measurements were performed by capturing a single GUV by a pair of optical tweezers, positioned at two opposite ends of the closed bilayer (**Fig. 6c**). In this configuration, by retaining the GUV, if the position of one optical trap was turned away, the elongation of the trapped GUV was induced. The maximum elongation of GUVs is achieved, when the trapping force, proportional to the trapping beam power, is equal to the GUV's restoring force. **Fig. 6d** reports the maximum relative elongation of GUVs obtained at different trapping laser power upon interaction with the amphiphilic gold nanoparticles, as well as for MUS-only gold nanoparticles and for GUV in aqueous condition. The consistently lower elongation with respect to the trapping beam power, as well as the decreased slope, observed in the case of MUS:OT gold nanoparticles suggests that the lipid bilayers of the GUVs are stiffer than GUVs incubated with no nanoparticles. Of note, there was no discernible decrease in elongation of GUVs incubated with MUS-only gold nanoparticles, suggesting that the amphiphilic character of the MUS:OT gold nanoparticles may play a role in the membrane stiffening. We suspect that in the case of the interaction of a CMLP with a cell, a relatively high local concentration of MUS:OT gold nanoparticles is presented to a portion of the plasma membrane, resulting in a locally stiffened region, which may allow for stabilization of the CMLP on the membrane. Such stabilization may also allow

for the clustering phenomenon observed over longer incubation times. Indeed, it has been shown that membrane stiffening can strongly hinder the endocytotic process, or even inhibit it. [48] (Saleem, Morlot et al. 2015) (Saleem, Morlot et al. 2015) [48] The additional PEGylation of one hemisphere of the CMLPs may further contribute to the particular membrane localization observed in this study.

Our studies were aimed at elucidating the importance of hierarchical surface patterns for particle interactions with plasma membranes in live cells. These particles decorated with MUS:OT gold nanoparticles and PEG exhibited the highest membrane-binding capacity, even at low particle concentrations. The marked differences between CMLPs and control particles, suggest selective affinity with plasma membranes which particles displaying standard gold nanoparticles do not have. Based on the GUV experiments, we further speculate that, after CLMPs adhere to the cellular membrane, the interaction of the amphiphilic gold NPs with the lipid bilayer induces a local stiffening of the cellular membrane itself which, in turn, inhibits the membrane engulfment needed to start the endocytotic pathway. With further work, cell membrane-localizing particles (CMLPs) may serve as a novel platform for intracellular delivery of payloads or as a research tool for investigating cell membrane phenomena.

Experimental Section

Materials. Poly(acrylamide-co-acrylic acid, sodium salts) (PAAm-*co*-AA) (MW 200 kD, 10% acrylic acid residues) was purchased from Polysciences (PA, USA). Amino dextran (MW 70 kD) was purchased from Molecular Probes (Oregon, USA). Rhodamine B isothiocyanate conjugated dextran (RITC-dextran, MW 70 kD) and fluorescein isothiocyanate conjugated dextran (FITC-dextran, MW 70 kD) were purchased from Sigma Aldrich. Acetylene-modified PAAm-*co*-AA was synthesized as described previously. [22] (Yoshida, Roh et al. 2009) (Yoshida, Roh et al. 2009) [22] Synthesis of azide-functionalized MUS:OT and control gold nanoparticles have been described previously by the

Stellacci group.[21] MDA-MB-231/GFP cells were obtained from Cell Biolabs, Inc. All cell culture materials were purchased from Invitrogen.

Fabrication of bicompartmental particles. The preparation of bicompartmental PAAm-*co*-AA particles was slightly modified from the method previously described. [25-27] (Roh, Martin et al. 2005, Roh, Martin et al. 2006, Roh, Yoshida et al. 2007) (Roh, Martin et al. 2005, Roh, Martin et al. 2006, Roh, Yoshida et al. 2007) [25-27] One solution was prepared by dissolving 50 mg PAAm-co-AA, 10 mg acetylene-modified PAAm-co-AA, and 2 mg of RITC-dextran in 1 mL of H_2O. The other jetting solution was made by dissolving 50 mg PAAm-co-AA, 10 mg amino-dextran, and 2 mg of FITC-dextran. Both solutions were stirred overnight. The prepared jetting solutions were loaded to two 1-mL syringes and set up side-by-side. A dual channel needle with two 26 gauge tips and 3.25 inch in length (FibriJets SA-0105, Micromedics, Inc., MN, USA) was connected to the syringes. The flow rates of the two solutions were simultaneously controlled by a single syringe pump (0.2–0.25 mL/h). A voltage around 15-18 kV was applied to the needles using a high potential generator (ES30P, Gamma High Voltage Research, Inc., USA) and the ground was connected to a piece of aluminium foil as a collecting substrate at a 30 cm distance from the end of needle. After EHD co-jetting, the particles were thermally crosslinked at 175 ^{o}C for 3 hrs. The final product was collected as a powder.

Surface modification of bicompartmental particles. 5 mg of bicompartmental particles and 20 mg of PEG-NHS were added to 0.5 mL H_2O and the mixture was stirred for 3 hrs. The suspension was centrifuged and the supernatant was removed. The particles were washed via two cycles of redispersion in fresh water and centrifugation. These particles were freeze-dried using a Labconco Freezone 4.5. After the washing procedure, 1 mg of N_3-functionalized Au NPs (isotropic for control, MUS:OT for CMLP), 0.2 mL of 0.03 M $CuSO_4$ (aq) and 0.2 mL H_2O was added to the PEGylated particles. Finally, 20 mg of sodium ascorbate was added and the suspension was agitated for 3 hrs. The mixture was centrifuged and the supernatant was removed. The residue was washed with water two times, 0.03 M $Na_2EDTA{\cdot}2H_2O$ (aq) three times, and water three times. The functionalized bicompartmental particles were collected after freeze-drying.

Particle characterization. An Olympus FluoView 500 Confocal Laser Scanning Microscopes (CLSM) was used to examine the compartmentalized fluorescence distributions of the bicompartmental particles prepared in this study. Ar/ArKr laser (λ = 488 nm) and GreNe laser (λ = 543 nm) were used to excite FITC and rhodamine B, respectively. The emission wavelength ranges collected were 508–523 nm for FITC and 580–595 nm for rhodamine B. Transmission electron microscopy (TEM, JEOL 3011) was employed for the microscopic imaging of bicompartmental particles using a copper TEM grid coated with a carbon film (400 meshes, Ted Pella). Cells were imaged by scanning electron microscopy (SEM) using an AMRAY 1910 Field Emission Scanning Electron Microscope.

Cell culture. MDA-MB-231/GFP cells were grown in Dulbecco's Modified Eagle Medium (DMEM) supplemented with 10% fetal bovine serum (FBS), 1X non-essential amino acids (NEAA), and 1X penicillin-streptomycin. All *in vitro* experiments were performed using cells that had been passaged no more than seven times.

In vitro particle incubation experiments. Cells were seeded at 50,000 cells/well on circular glass slides in 12-well plates and incubated at 37 ^{o}C overnight. Media was exchanged with particles in media at a given concentration, and incubated at 37 ^{o}C for a designated amount of time. After incubation, cells were washed with PBS 2-3x, and then fixed with either 4% paraformaldehyde (for confocal) or 2.5% glutaraldehyde (for SEM) for 30 min. For confocal, glass slides were washed with PBS once more, mounted with ProLong Gold, and subsequently imaged using the Olympus CLSM. Triplicate incubations were performed, obtaining confocal images from each incubation – for analysis, incubations were considered where at least 100 cells were analyzed for each condition (for each type of particle and concentration). For SEM, cell samples were prepared after glutaraldehyde fixing by sequential ethanol washing – cells were incubated sequentially with 10%, 30%, 50%, 70%, 90% (2x), and 100% (2x) ethanol in water solutions for 5-10 min at each concentration. Cells were then washed and incubated with HMDS; HMDS was exchanged twice after 5-10 min intervals and the

final HMDS was allowed to evaporate overnight in a laminar flow hood. Cell samples were then gold sputter-coated and imaged using the AMRAY SEM.

K-means analysis. The red fluorescence channel images from the incubation experiments, a representative from each concentration and incubation time period, were imported into MATLAB and used to estimate the positions of the particles using imfindcircles(). The built-in function kmeans() was employed to determine k-means clustering solutions, and the optimal number of clusters k was determined by the k-means solution with the highest average silhouette number as given by silhouette() (K-means was evaluated for the number of clusters from 2 to 25).

GUV preparation. GUVs used for Raman analysis were prepared by electroformation, essentially following the procedure described in ref. [49]. Briefly, 1,2-dioleoyl-sn-glycero-3-phosphocholine (DOPC, by Avanti) dissolved in a 10:1 chloroform to methanol solution was spread over the conducting side of an indium tin oxide (ITO) slide and dessiccated under reduced pressure. Therefore, a capacitive cell was formed with a second ITO slide and teflon strips acting as spacers. The chamber was finally filled with distilled water and a sine wave (1.5 V, 10 Hz) was applied to the electroformation chamber for 2 h. This procedure produces GUVs which can be stored for up to two weeks at room temperature. For stretching measurements, the electroformation chamber was filled with a 0.3 M sucrose solution and the formed GUVs, filled with the sucrose solution, were diluted into a 0.37 M glucose solution. The refractive index mismatch between sucrose and glucose solutions allows an optimal GUVs imaging under bright field illumination. Moreover, the contrast of the index of refraction across the lipid bilayer allows an efficient optical trapping and pulling of the membrane. For both Raman and stretching measurements, we selected vesicles with a diameter ~ 10 μm.

Raman Tweezers system. GUV investigation presented herein performed by using a combined Optical Tweezers and micro-Raman system (Raman Tweezers). The set-up has been described in detail elsewhere.[50] Briefly, it consists essentially in a home-made inverted microscope, endowed with a trapping beam (Nd:YAG, 1064 nm, Ventus 1064) and a Raman probe at 532 nm (Spectra Physics Millennia Xs). The microscope is equipped with a 100X objective lens (Olympus oil-immersion

infinity corrected objective, 1.4 N.A.), in which both lasers are injected through a dichroic mirror. By using a galvomirror, the trapped object is moved across the confocal detection volume of the Raman probe. For stretching measurements, a double-trap system (*optical stretcher*) is set up by applying a square voltage signal at a frequency of 1 kHz to a galvomirror, placed on the optical path of the trapping beam. This allows an easy and optimal control of the relative distance between the two optical traps.

Raman measurements on DOPC GUVs. Raman analysis was performed on DOPC-GUVs incubated for three hours with MUS:OT NPs. Measurements have been carried out at three different nanoparticles concentrations: 0.01 mg/ml, 0.1 mg/ml and 1mg/ml.

From this analysis, it comes out that, starting from a concentration level of 0.1 mg/ml, a significant number of GUVs spectra exhibit new spectral signatures clearly due to MUS:OT NPs, as shown in Fig. S4a. As a matter of facts, while the spectrum in panel *i)* shows spectral features mainly arising from vibrations of the DOPC hydrocarbon chains, the spectrum reported in panel *ii)* clearly exhibits new features, mainly around 986 cm^{-1} and 1613 cm^{-1}, likely due to sulphate and CC bonds in MUS:OT NPs, respectively. However, a high degree of heterogeneity of the acquired spectra shows up, in terms of the relative intensity of bands due to DOPC and MUS:OT NPs. A quantitative description of this process has been obtained by evaluating the ratio $R=I_{986}/I_{1445}$ of the sulphate band intensity against the DOPC band intensity at 1445 cm^{-1} for 60 GUVs exposed to nanoparticles at a concentration of 1 mg/ml. The result is shown in Fig. S4b. This clearly suggests a random accumulation process of NPs near/inside the lipid bilayer. Importantly, as shown in Fig. 6a, the intensity of DOPC Raman features remains reasonably unaffected by NPs addiction and NPs-related bands appear to be simply *added* to the DOPC features, with no evidence of lipid chains destucturation typically mirrored, from a spectral point of view, by a reduction in intensity and a broadening of the lipid features. This further supports our evidence of a

complete bio-compatibility of the amphiphilic gold nanoparticles under the investigated concentration range.

GUVs stretching measurements. To check the effect of the amphiphilic gold nanoparticles on the micromechanical properties of GUVs, we proceeded by capturing a single GUV by a pair of OTs, positioned at two opposite ends of the closed bilayer (Fig. 6c). Therefore, we increased the distance between the two optical traps up to the maximum extent possible at the given power of the trapping laser. In this condition, the elastic stretching force exerted on the GUVs by the Optical Tweezers balances the GUV restoring force. Therefore, we gradually increased the laser power, proportional to the force applied to the membrane, from 20 mW to 120 mW. At each step, a GUV image was acquired, successively processed by ImageJ software for the estimation of the GUV relative elongation.

In Fig. 6d we report the relative axial elongation versus the Optical Tweezers laser power for measurements on 10 GUVs upon 3 hours incubation with MUS:OT nanoparticles (1 mg/ml), incubation with MUS nanoparticles (1 mg/ml) as well as for GUVs in aqueous solution. Clearly, the lower slope obtained for the first case indicates an increase of the apparent membrane stretching constant, and, therefore, a membrane stiffening induced by MUS-OT nanoparticles. On the contrary, interaction with MUS nanoparticles seems not to affect the GUVs mechanical properties (Fig. 6d).

Supporting Information

Supporting Information is available from the Wiley Online Library or from the author.

Acknowledgments

The authors would like to acknowledge funding from the European Community's Seventh Framework Programme (FP7/2007-2013) under grant agreement nº 310445 (SAVVY), and

the Defense Threat Reduction Agency (DTRA) for funding provided through grant HDTRA1-15-1-0045.

Author Contributions

Tae-Hong Park prepared and characterized all polymeric particles used in the study. The gold nanoparticles were synthesized by Randy P. Carney. Asish C Misra performed all *in vitro* experiments, corresponding confocal & electron microscopy, and K-means analysis. Giulia Rusciano performed all GUV experiments. The experiments were designed by Tae-Hong Park and Asish C Misra, with advice from Francesco Stellacci and Joerg Lahann.

References

(1) Alarcon, C. D. H.; Pennadam, S.; Alexander, C. *Chem Soc Rev* **2005**, *34*, 276.
(2) Dykman, L.; Khlebtsov, N. *Chem Soc Rev* **2012**, *41*, 2256.
(3) Li, Z. X.; Barnes, J. C.; Bosoy, A.; Stoddart, J. F.; Zink, J. I. *Chem Soc Rev* **2012**, *41*, 2590.
(4) Liu, X. Y.; Chu, P. K.; Ding, C. X. *Mat Sci Eng R* **2004**, *47*, 49.
(5) Neuberger, T.; Schopf, B.; Hofmann, H.; Hofmann, M.; von Rechenberg, B. *J Magn Magn Mater* **2005**, *293*, 483.
(6) Niinomi, M. *Metall Mater Trans A* **2002**, *33*, 477.
(7) Cho, K.; Wang, X.; Nie, S.; Chen, Z. G.; Shin, D. M. *Clin Cancer Res* **2008**, *14*, 1310.
(8) Nie, Z.; Petukhova, A.; Kumacheva, E. *Nat Nanotechnol* **2010**, *5*, 15.
(9) Shi, J.; Votruba, A. R.; Farokhzad, O. C.; Langer, R. *Nano Lett* **2010**, *10*, 3223.
(10) Soppimath, K. S.; Aminabhavi, T. M.; Kulkarni, A. R.; Rudzinski, W. E. *J Control Release* **2001**, *70*, 1.
(11) Lidmar, J.; Mirny, L.; Nelson, D. R. *Phys Rev E* **2003**, *68*.
(12) Glotzer, S. C.; Solomon, M. J. *Nature materials* **2007**, *6*, 557.
(13) Douglas, T.; Young, M. *Science* **2006**, *312*, 873.
(14) Glotzer, S. C.; Horsch, M. A.; Iacovella, C. R.; Zhang, Z. L.; Chan, E. R.; Zhang, X. *Curr Opin Colloid In* **2005**, *10*, 287.
(15) Hoekstra, D.; Kok, J. W. *Bioscience Rep* **1989**, *9*, 273.
(16) Yoon, J.; Lee, K. J.; Lahann, J. *J Mater Chem* **2011**, *21*, 8502.
(17) Lee, K. J.; Yoon, J.; Lahann, J. *Curr Opin Colloid In* **2011**, *16*, 195.
(18) Misra, A. C.; Bhaskar, S.; Clay, N.; Lahann, J. *Adv Mater* **2012**, *24*, 3850.

(19) Saha, S.; Copic, D.; Bhaskar, S.; Clay, N.; Donini, A.; Hart, A. J.; Lahann, J. *Angew Chem Int Edit* **2012**, *51*, 660.
(20) Lee, K. J.; Yoon, J.; Rahmani, S.; Hwang, S.; Bhaskar, S.; Mitragotri, S.; Lahann, J. *P Natl Acad Sci USA* **2012**, *109*, 16057.
(21) Bhaskar, S.; Pollock, K. M.; Yoshida, M.; Lahann, J. *Small* **2010**, *6*, 404.
(22) Yoshida, M.; Roh, K. H.; Mandal, S.; Bhaskar, S.; Lim, D. W.; Nandivada, H.; Deng, X. P.; Lahann, J. *Advanced Materials* **2009**, *21*, 4920.
(23) Roh, K. H.; Lahann, J. *Abstr Pap Am Chem S* **2007**, *233*.
(24) Yoshida, M.; Roh, K. H.; Lahann, J. *Biomaterials* **2007**, *28*, 2446.
(25) Roh, K. H.; Yoshida, M.; Lahann, J. *Langmuir* **2007**, *23*, 5683.
(26) Roh, K. H.; Martin, D. C.; Lahann, J. *Nat Mater* **2005**, *4*, 759.
(27) Roh, K. H.; Martin, D. C.; Lahann, J. *J Am Chem Soc* **2006**, *128*, 6796.
(28) Roh, K. H.; Yoshida, M.; Lahann, J. *Materialwiss Werkst* **2007**, *38*, 1008.
(29) Bhaskar, S.; Roh, K. H.; Jiang, X. W.; Baker, G. L.; Lahann, J. *Macromolecular rapid communications* **2008**, *29*, 1973.
(30) Sarangi, N. K.; Patnaik, A. *Rsc Adv* **2014**, *4*, 29463.
(31) Gao, Y.; Yu, Y. *J Am Chem Soc* **2013**, *135*, 19091.
(32) Li, B. H.; Wang, M.; Chen, K.; Cheng, Z. F.; Chen, G. J.; Zhang, Z. X. *Macromol Rapid Comm* **2015**, *36*, 1200.
(33) Bartolami, E.; Bouillon, C.; Dumy, P.; Ulrich, S. *Chem Commun* **2016**, *52*, 4257.
(34) Ganan-Calvo, A. M. *Phys Rev Lett* **1997**, *79*, 217.
(35) Luedtke, W. D.; Landman, U.; Chiu, Y. H.; Levandier, D. J.; Dressler, R. A.; Sok, S.; Gordon, M. S. *J Phys Chem A* **2008**, *112*, 9628.
(36) Lahann, J. *Small* **2011**, *7*, 1149.
(37) Verma, A.; Uzun, O.; Hu, Y.; Hu, Y.; Han, H. S.; Watson, N.; Chen, S.; Irvine, D. J.; Stellacci, F. *Nat Mater* **2008**, *7*, 588.
(38) Van Lehn, R. C.; Ricci, M.; Silva, P. H.; Andreozzi, P.; Reguera, J.; Voitchovsky, K.; Stellacci, F.; Alexander-Katz, A. *Nat Commun* **2014**, *5*, 4482.
(39) Yang, Y. S.; Carney, R. P.; Stellacci, F.; Irvine, D. J. *ACS Nano* **2014**, *8*, 8992.
(40) Atukorale, P. U.; Yang, Y. S.; Bekdemir, A.; Carney, R. P.; Silva, P. J.; Watson, N.; Stellacci, F.; Irvine, D. J. *Nanoscale* **2015**, *7*, 11420.
(41) Van Lehn, R. C.; Atukorale, P. U.; Carney, R. P.; Yang, Y. S.; Stellacci, F.; Irvine, D. J.; Alexander-Katz, A. *Nano Lett* **2013**, *13*, 4060.
(42) Panyam, J.; Sahoo, S. K.; Prabha, S.; Bargar, T.; Labhasetwar, V. *Int J Pharm* **2003**, *262*, 1.
(43) Bray, D.; Levin, M. D.; Morton-Firth, C. J. *Nature* **1998**, *393*, 85.
(44) Gajate, C.; Mollinedo, F. *J Biol Chem* **2005**, *280*, 11641.
(45) Richmond, D. L.; Schmid, E. M.; Martens, S.; Stachowiak, J. C.; Liska, N.; Fletcher, D. A. *P Natl Acad Sci USA* **2011**, *108*, 9431.
(46) Dholakia, K.; Cizmar, T. *Nat Photonics* **2011**, *5*, 335.
(47) Schulz, M.; Olubummo, A.; Binder, W. H. *Soft Matter* **2012**, *8*, 4849.
(48) Saleem, M.; Morlot, S.; Hohendahl, A.; Manzi, J.; Lenz, M.; Roux, A. *Nature Communications* **2015**, *6*.
(49) Poole, C. & Losert, W. *Methods in Molecular Biology* **2007**, 400.
(50) De Luca, A.C., Rusciano, G., Ciancia, R., Martinelli, V., Pesce, G., Rotoli, B. & A. Sasso. *Opt. Express* **2008**, *16*, 7943-7957.

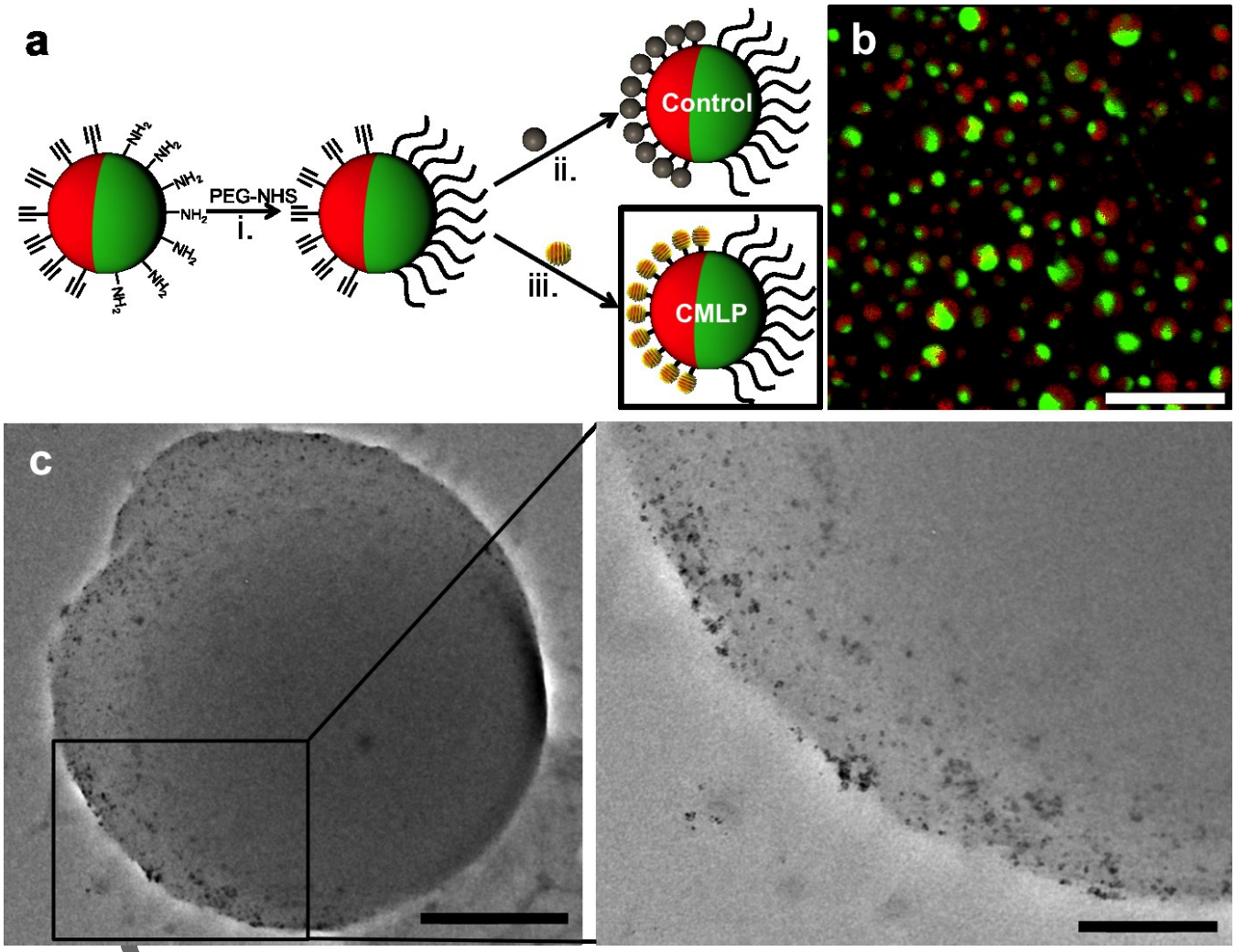

Figure 1 | Fabrication and characterization of hierarchically-assembled particles. (a) Design and synthesis scheme of control particles and cell membrane localizing particles, CMLPs. (b) Fluorescent CLSM overlay image of CMLPs demonstrating their bicompartmental architecture. Scale bar is 20 μm. (c) TEM image of a CMLP (with a magnified image of it on the right), showing selective surface modification with MUS:OT gold nanoparticles on one hemisphere. Scale bars are 500 nm for the left TEM image, and 200 nm for the right TEM image.

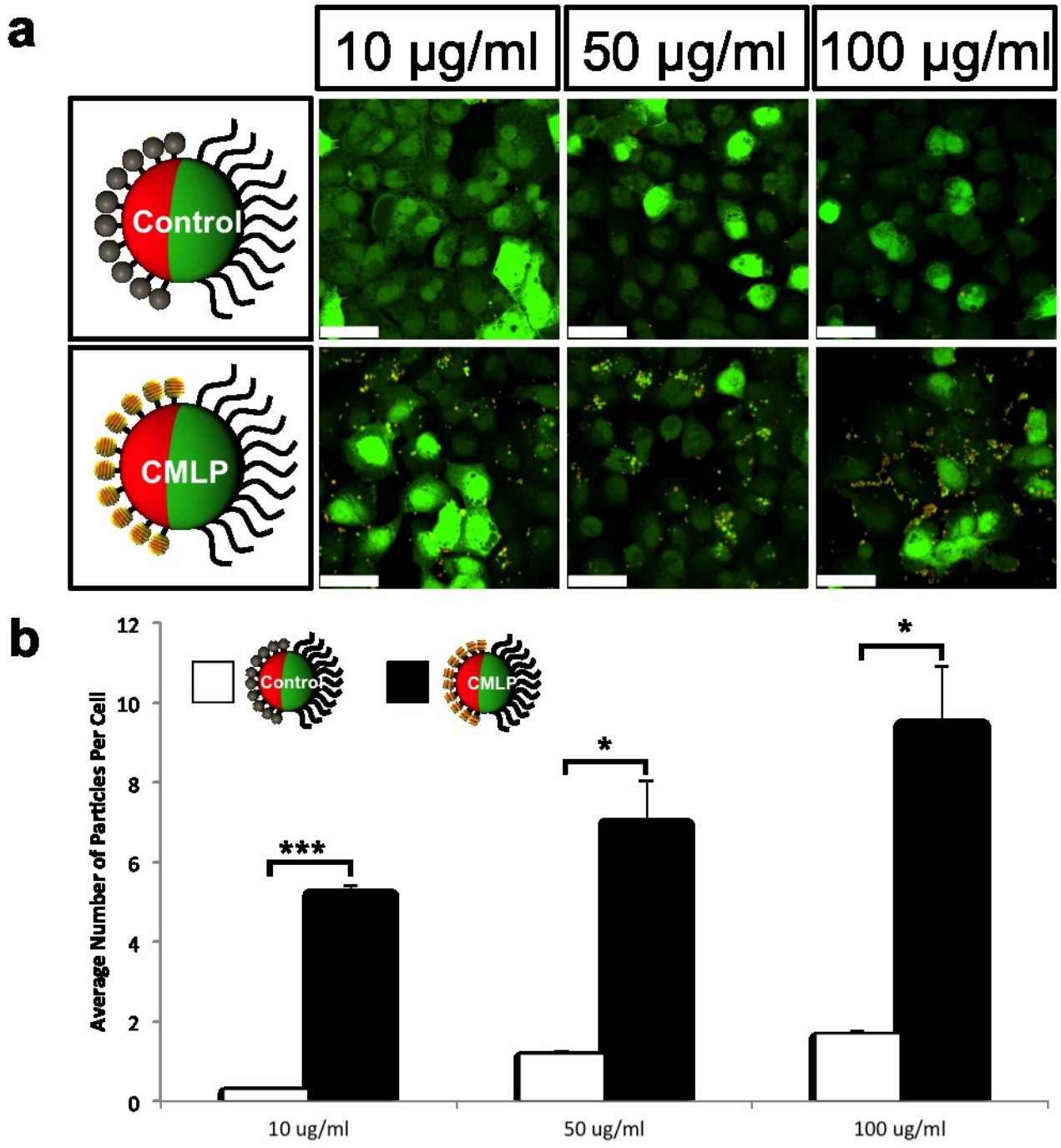

Figure 2 | Particle incubation with MDA-MB-231/GFP cells. (a) Fluorescent CLSM overlay images of MDA-MB-231/GFP cells incubated with control particles and CMLPs for 6 hours at concentrations of 10, 50, and 100 µg/ml. Scale bars are 50 µm. (b) Quantification of average number of bound and/or internalized particles per cell for 6-hour incubation experiments (Fig. 2). Significance levels are: * $p < 0.01$, ** $p < 0.001$, *** $p < 0.0001$

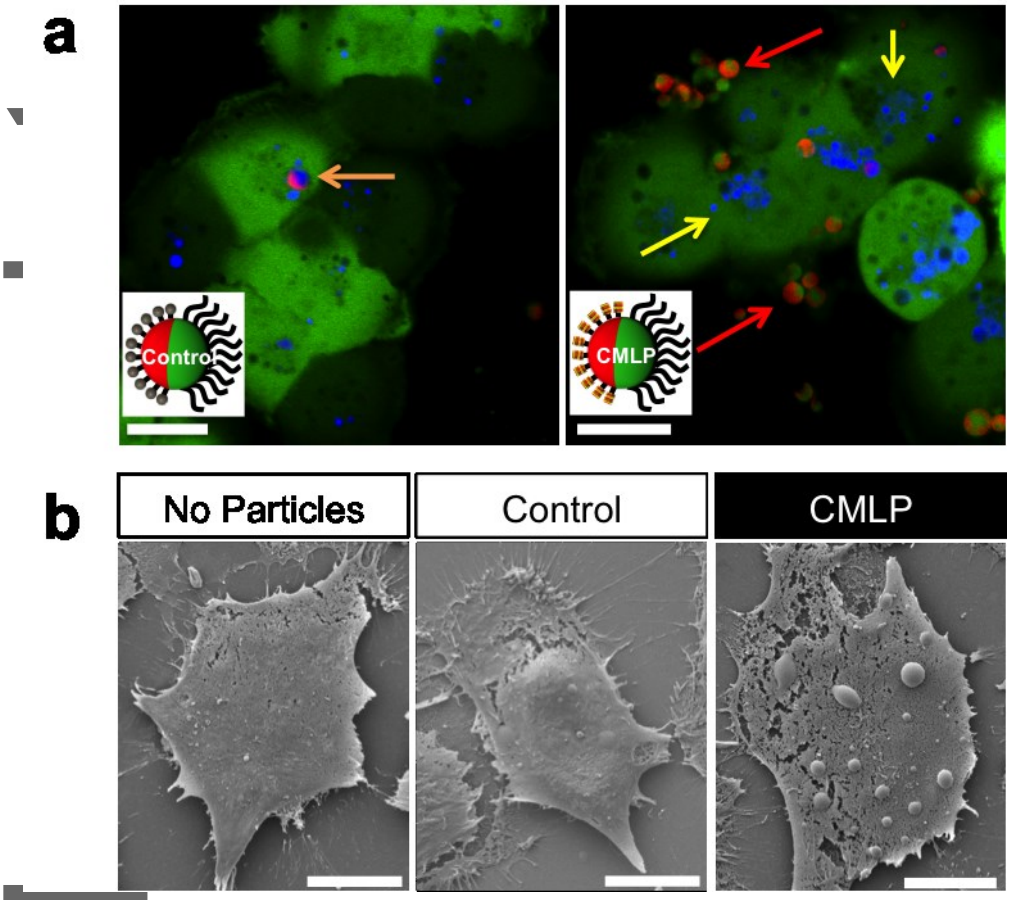

Figure 3 | Investigation of *in vitro* binding. (a) Fluorescent CLSM images from endosomal staining studies where 10 µg/ml of particles (red & green) were incubated with MDA-MB-231/GFP cells (green) for 6 hours, followed by endosomal staining (blue). Scale bars are 10 µm. (b) SEM images of MDA-MB-231/GFP cells after incubation with 10 µg/ml of particles. Scale bars are 20 µm.

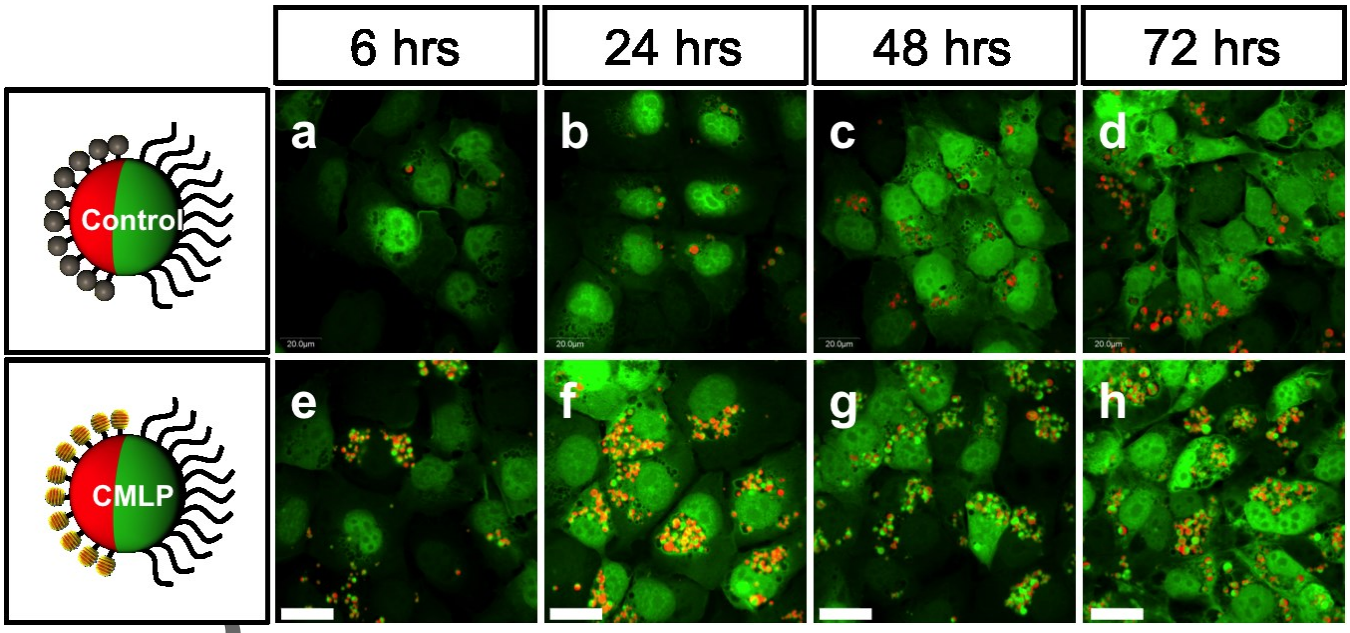

Figure 4 | Longer-term behavior. Representative fluorescent CLSM overlay images from long-term incubation studies with control particles (a-d) and CMLPs (e-h) at a fixed concentration of 100 μg/ml, with incubation times of 6 (a, e), 24 (b, f), 48 (c, g), and 72 (d, h) hours. Scale bars are 25 μm.

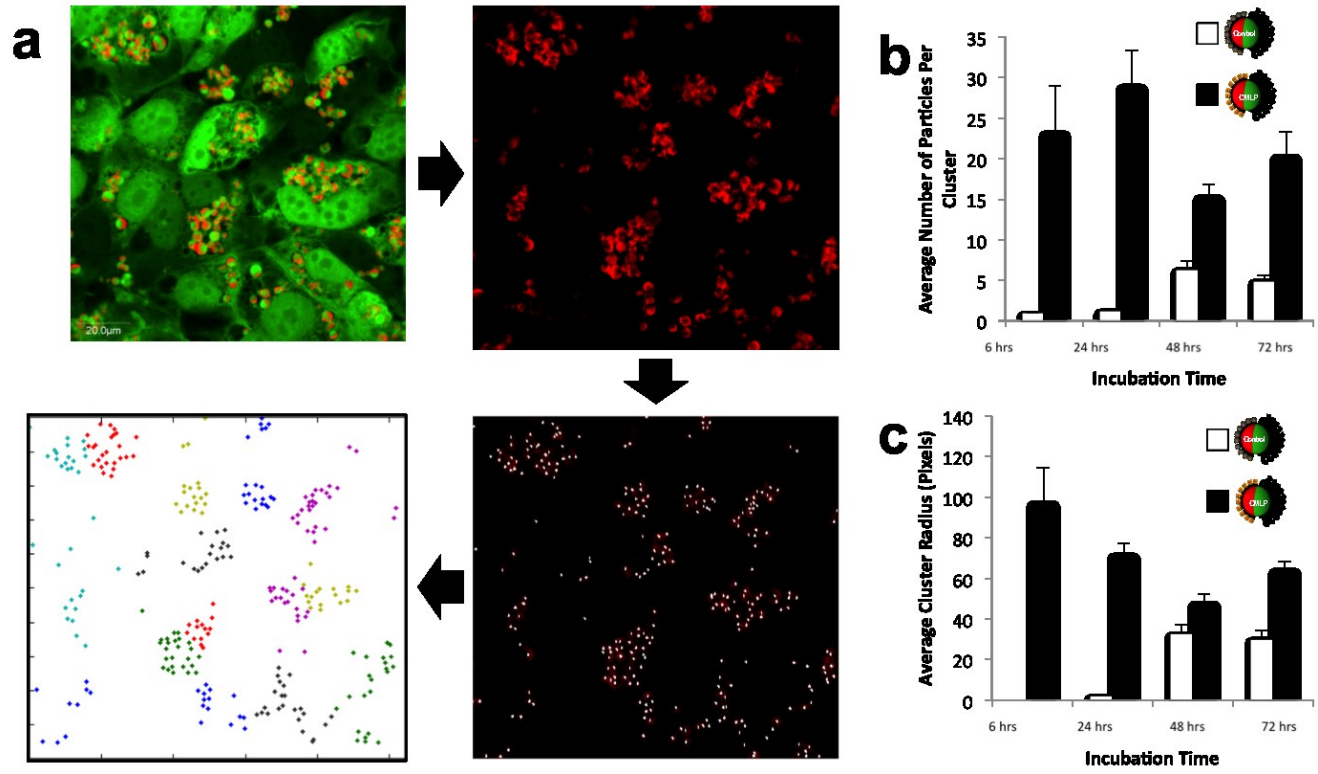

Figure 5 | Clustering Analysis. (a) K-means clustering analysis of particles at different incubation times, obtained by determining particle position from estimating centers of particles via extracted red fluorescence images. (b) Average number of particles per cluster and (c) average cluster radius. Black bars – CMLPs, white bars – control particles. Note average cluster radius for control particles at 6 hrs is 0 as each cluster contains 1 particle. Error bars are standard error.

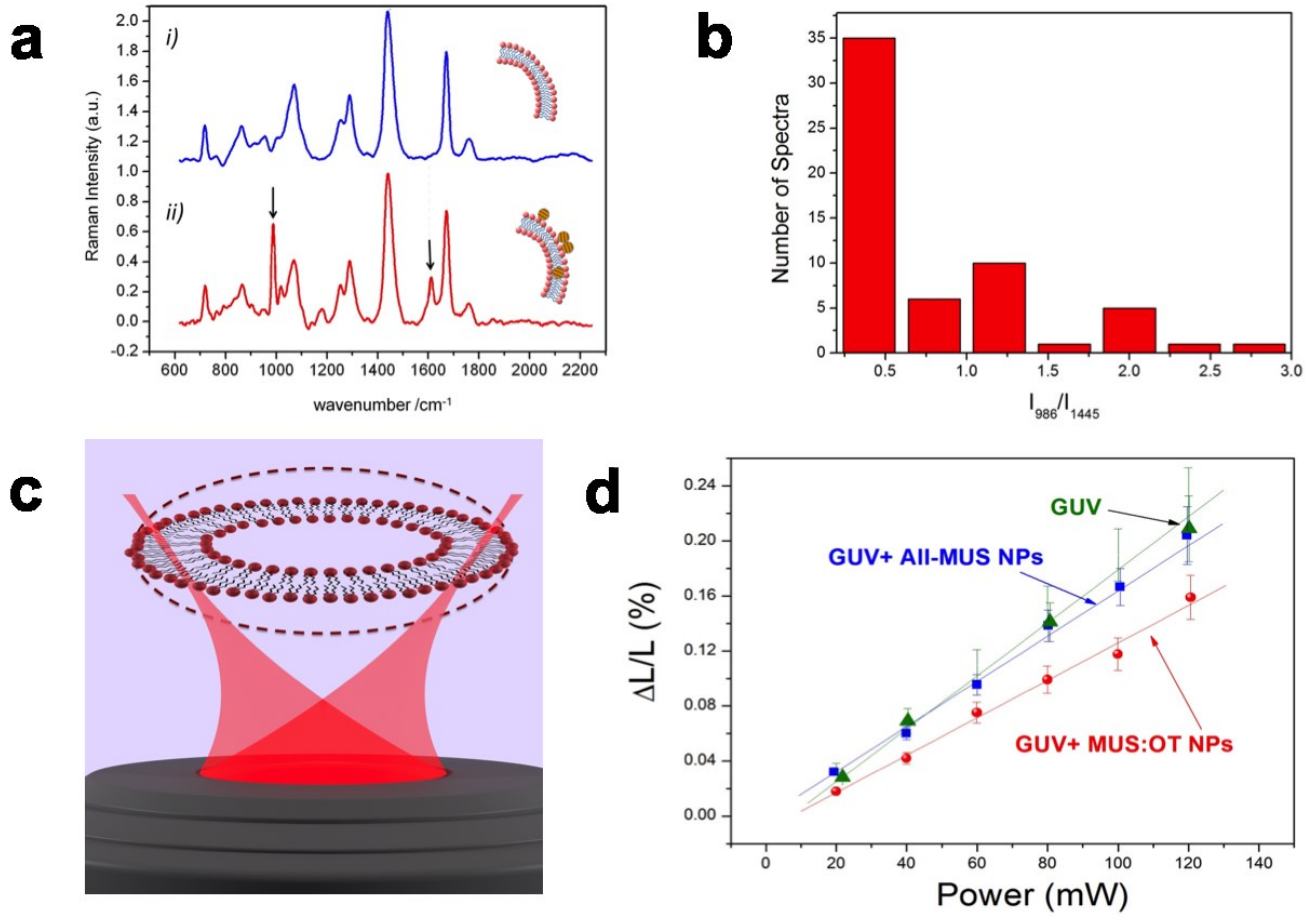

Figure 6 | Individual gold nanoparticle interactions with GUVs. (a) Raman spectra of a single GUV (*i*) in aqueous solution or (*ii*) under incubation with MUS:OT NPs at a 1 mg/ml concentration. The arrows in panel *ii)* highlight two features related to MUS:OT NPs. (b) Statistical distribution of the ratio $R=I_{986}/I_{1445}$ for 60 GUVs exposed to MUS:OT gold nanoparticles for three hours. (c) Cartoon of the stretching process of a single GUV induced by two optical traps, or tweezers. (d) Relative GUV elongation *versus* optical tweezer laser power for *i)* GUVs exposed to MUS:OT gold nanoparticles (MUS:OT NPs), *ii)* GUVs exposed to MUS-only gold nanoparticles (All-MUS NPs), *iii)* GUVs in aqueous solution. Errors bars correspond to the standard deviation for measurements on 10 GUVs.

Table of Contents

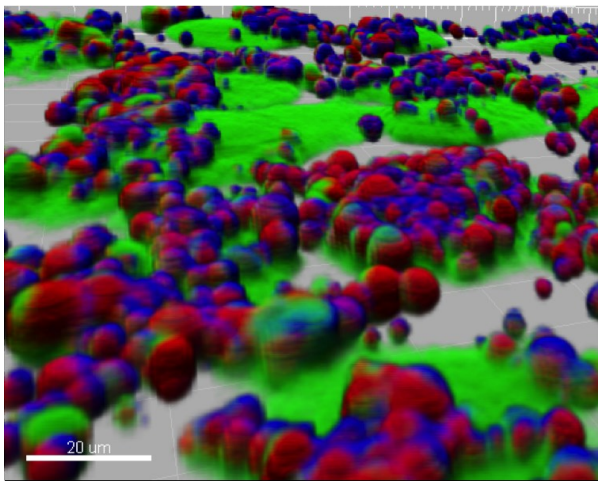

Assemblies of polymer-based carrier particles with amphiphilic gold nanoparticles selectively immobilized on one hemisphere are shown to selectively localize to the plasma membranes of mammalian cells, as shown above.